

# Power and spectral index anisotropy of the entire inertial range of turbulence in the fast solar wind

R. T. Wicks,<sup>1\*</sup> T. S. Horbury,<sup>1</sup> C. H. K. Chen<sup>1</sup> and A. A. Schekochihin<sup>2</sup>

<sup>1</sup>*Space and Atmospheric Physics Group, Imperial College London, London SW7 2AZ*

<sup>2</sup>*Rudolf Peierls Centre for Theoretical Physics, University of Oxford, Oxford OX1 3NP*

Accepted 2010 June 7. Received 2010 May 20; in original form 2010 February 10

## ABSTRACT

We measure the power and spectral index anisotropy of magnetic field fluctuations in fast solar wind turbulence from scales larger than the outer scale down to the ion gyroscale, thus covering the entire inertial range. We show that the power and spectral indices above the outer scale of turbulence are approximately isotropic. The turbulent cascade causes the power anisotropy at smaller scales manifested by anisotropic scalings of the spectrum: close to  $k^{-5/3}$  across and  $k^{-2}$  along the local magnetic field, consistent with a critically balanced Alfvénic turbulence. By using data at different radial distances from the Sun and calculating the radial dependence of the ratio of the outer scale to the ion gyroscale, we show that the width of the inertial range does not change with heliocentric distance. At the smallest scales of the inertial range, close to the ion gyroscale, we find an enhancement of power parallel to the magnetic field direction coincident with a decrease in the perpendicular power. This is most likely related to energy injection by ion kinetic modes such as the firehose instability and also marks the beginning of the kinetic range, sometimes called the dissipation range, of solar wind turbulence.

**Key words:** instabilities – MHD – plasmas – turbulence – solar wind.

## 1 INTRODUCTION

The magnetic field embedded in the turbulent solar wind (Goldstein, Roberts & Matthaeus 1995) causes several kinds of anisotropy. Different physical processes operate parallel and perpendicular to this field. The fluctuations (with respect to the large-scale mean field) of the parallel and perpendicular components of the magnetic field scale differently from large (Nicol, Chapman & Dendy 2009) to small scales (Alexandrova et al. 2008; Sahraoui et al. 2009). Several solar wind quantities, e.g. cross-helicity (Milano et al. 2004), magnetic field correlation function (Dasso et al. 2005; Osman & Horbury 2007; Weygand et al. 2009) and velocity components (Chapman & Hnat 2007), vary anisotropically with respect to the mean magnetic field direction.

Recent advances in the study of the solar wind have shown that the magnetic field causes spatial anisotropy in the properties of the fluctuating fields along and across the local mean field direction. This anisotropy can be measured in correlation functions (Matthaeus et al. 1994), power (Bieber, Wanner & Matthaeus 1996; Chen et al. 2010b) and variation of the spectral index depending on the angle to the local mean field (Horbury, Forman & Oughton 2008; Podesta 2009; Chen et al. 2010b); see Chen et al. (2010a) for a discussion of the relationship between these manifestations of the anisotropy.

These results have shown that the measured power spectra of the turbulent magnetic field at different angles to the local mean field are consistent with those predicted by the phenomenological theory of Goldreich & Sridhar (1995) based on the conjecture of critical balance between linear (Alfvén) and non-linear time-scales in the turbulent cascade. It is important to remark, however, that the Goldreich & Sridhar (1995) theory only applies to balanced turbulence so that an appropriate generalization of this theory is required for the description of imbalanced solar wind turbulence, such as that seen here in the fast solar wind. The problem of anisotropic scaling in imbalanced turbulence is unsolved and there are several competing theories (e.g. Lithwick, Goldreich & Sridhar 2007; Chandran 2008; Beresnyak & Lazarian 2009; Perez & Boldyrev 2009).

Observational studies have focused on the inertial range, the small-scale boundary of which is defined by the scale at which kinetic effects become important, and have not approached the large-scale limit, the outer scale, the point at which the power spectrum  $k^\alpha$  rolls over to a flatter index of  $\alpha \approx -1$  (e.g. Horbury et al. 1996). Here we extend the wavelet-based local magnetic field analysis of Horbury et al. (2008) and Podesta (2009) to larger scales, including the outer scale. We investigate the properties of the turbulence, in particular the anisotropy, across the entire inertial range and demonstrate for the first time the development of the cascade from its original, nearly isotropic, state at low frequencies all the way down to its final, anisotropic, state near the ion gyroscale.

\*E-mail: r.wicks@imperial.ac.uk

## 2 WAVELETS AND THE LOCAL MEAN MAGNETIC FIELD

We use the method devised by Horbury et al. (2008) and detailed by Podesta (2009). The Morlet wavelet is used to obtain the power in magnetic field fluctuations as a function of both frequency and time. Neighbouring wavelet scales differ by a factor of 1.6, approximately the uncertainty on the frequency resolution of the Morlet wavelet; this ensures coverage of frequency without oversampling (Torrence & Compo 1998). The scale of the wavelet envelope function (a Gaussian) is used as the length over which to calculate the mean magnetic field direction (Horbury et al. 2008). This results in a mean field local to the fluctuation and not the larger scale field often considered in other studies (e.g. Tessein et al. 2009). The power calculated using the wavelet is then assigned to a bin corresponding to an angle  $\theta_B$  between the local field and the radial direction (the solar wind flows radially past the spacecraft) and a Fourier frequency  $f$  associated with the wavelet scale, giving  $P(f, \theta_B)$ . We adopt the Taylor hypothesis (Taylor 1938): when the flow speed is much greater than the sound and Alfvén speeds, a time series can be considered to be a 1D cut through a time stationary plasma. We take periods of Ulysses data from 1995, when the spacecraft was in fast polar solar wind. We use 1-s resolution Ulysses magnetic field data (Balogh et al. 1992); data gaps are linearly interpolated but are rare, accounting for approximately 6 per cent of the data. Analysing each period produces a power spectrum ranging in spacecraft frequency  $f$  between  $3.3 \times 10^{-5}$  and  $2.5 \times 10^{-1}$  Hz. We resolve  $\theta_B$  in  $10^\circ$  bins between  $0^\circ$  and  $90^\circ$ . For all of the periods studied here, the global average Parker field points away from the Sun with an angle between  $20^\circ$  and  $45^\circ$  to the radial direction. At the highest frequencies there are  $\sim 10^4$  power measurements in each  $(f, \theta_B)$  bin. At the lowest frequencies,  $\theta_B$  tends to the angle expected from the Parker spiral and bins typically contain  $\sim 10$  observations; any bin with fewer than five points is rejected.

Ulysses observations are made at 1-s cadence; however, the important physical scale for kinetic plasma physics in the solar wind is the proton gyroscale  $\rho_i$ . In order to compare different periods directly and to cast our results in physically relevant units, we convert the spacecraft observation frequency into a flow-parallel wavenumber  $k$  by dividing by the average solar wind speed  $|V|$  and normalize this by  $\rho_i$ :

$$k\rho_i = \frac{2\pi f \rho_i}{|V|} = \frac{2\pi f \sqrt{2k_B T_i m_i}}{e|V||B|}, \quad (1)$$

where  $k_B$  is Boltzmann's constant,  $T_i$  is the proton temperature,  $m_i$  is the mass of a proton,  $e$  is the charge on a proton and  $|B|$  is the magnetic field strength.

## 3 ANISOTROPY OF THE ENTIRE INERTIAL RANGE

First, we analyse a period of fast polar wind from Ulysses data between days 100 and 200 of 1995; during this time Ulysses moved from a solar latitude of  $28^\circ$  to  $79^\circ$  and distance of 1.38 to 1.93 au. Such a long interval is necessary to obtain an anisotropic power spectrum at the lowest frequencies used here; shorter periods can be used if angular resolution is not required at such low frequencies. Fig. 1 shows the trace of the magnetic field power tensor, averaged over periods when the solar wind flow is parallel,  $P_{\parallel}(0^\circ \leq \theta_B < 10^\circ)$  and perpendicular,  $P_{\perp}(80^\circ \leq \theta_B < 90^\circ)$  to the local magnetic field calculated using wavelets. We also show the average Fourier power for the same period. At the smallest values of  $k\rho_i$ , the power is

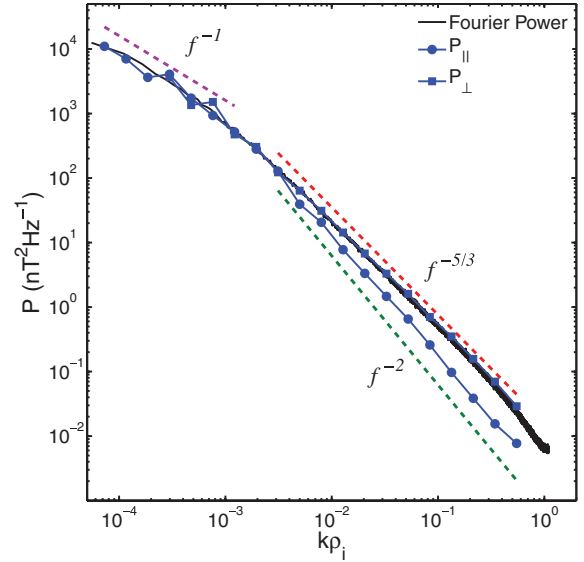


**Figure 1.** Trace of the wavelet and Fourier power spectra of magnetic field observations from Ulysses for the period between days 100 and 200 of 1995. Frequencies are converted to wavenumbers using the solar wind velocity and normalized to the ion gyroradius  $\rho_i$  (equation 1). See Fig. 4 for compensated spectra.

isotropic and all three lines lie close together with a spectral index of approximately  $-1$ . At  $k\rho_i \approx 3 \times 10^{-3}$ ,  $P_{\parallel}$  begins to diverge from the Fourier power and  $P_{\perp}$ . The power anisotropy increases as  $k\rho_i$  increases;  $P_{\perp}$  and the Fourier power follow each other closely and are a factor of 5 larger than  $P_{\parallel}$  at the largest  $k\rho_i$  measured. We stress that the use of wavelets to analyse the anisotropy of the magnetic field means that the magnetic field is not broken into components parallel and perpendicular to the mean field. Thus the terms  $P_{\parallel}$  and  $P_{\perp}$  do not refer to components of the field but to the mean trace power in the field when the flow past the spacecraft is parallel or perpendicular to the mean field.

In Fig. 2, we show the dependence of spectral index  $\alpha$  on scale;  $\alpha$  is determined by a least-squares fitting in log space of a straight

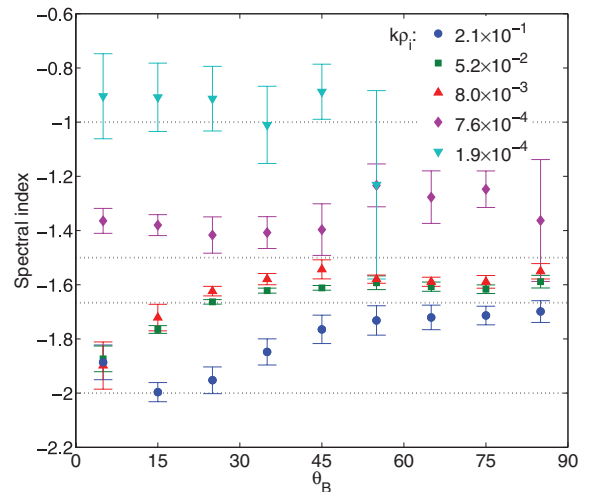


**Figure 2.** Dependence of the spectral index in different scale ranges on angle to the local mean magnetic field direction. The error bars are calculated from the residuals of linear least-squares fitting of straight lines to  $\log(P)$  versus  $\log(k\rho_i)$ .

line to power measurements. Each fit uses five wavelet power measurements covering scales separated by a factor of 10.5. The  $k\rho_i$  shown are the central values of each window. At large scales ( $k\rho_i = 1.9 \times 10^{-4}$ ), the spectra have an isotropic spectral index  $\alpha \approx -1$ . Above  $k\rho_i \approx 5 \times 10^{-4}$  (diamonds in Fig. 2), the spectrum steepens. As  $k\rho_i$  increases, the spectral indices decrease further and their values vary with  $\theta_B$  but only slowly with scale (squares and triangles in Fig. 2). These scales show a similar result to those of Horbury et al. (2008) and Podesta (2009) and confirm that in the inertial range fluctuations have a parallel spectral index of  $-2$ , while the perpendicular spectral index lies between the  $-5/3$  of a critically balanced Alfvénic cascade (Goldreich & Sridhar 1995) and the  $-3/2$  predicted by the theory of dynamically aligned Alfvénic turbulence (Boldyrev 2006). We will show in the next section that the data, in general, support a value closer to  $-5/3$ .

At the largest values of  $k\rho_i$  (blue circles in Fig. 2), the spectral index decreases compared to the inertial range for all  $\theta_B > 10^\circ$  and a value close to  $-2$  is found for a wider range of  $\theta_B$ . This is the beginning of the effect of kinetic physics close to the ion gyroscale (e.g. Schekochihin et al. 2009), as we show in the next section. Thus, we have covered the entire inertial range of magnetohydrodynamic turbulence, from the effective outer scale, defined as the point in the spectrum at low wavenumbers where measurable changes or deviations from the inertial range scaling occur, to the beginning of kinetic effects at the ion gyroscale.

#### 4 DEPENDENCE ON HELIOCENTRIC DISTANCE

As the solar wind travels away from the Sun,  $\rho_i$  increases,  $|B|$  decreases, the collisional and turbulent ages of the plasma increase and the outer scale moves to lower frequencies. Here we perform the same analysis as in the previous section for five 50-d periods of Ulysses data from 1995, taken at different distances from the Sun and so investigate the dependence on heliocentric distance of the anisotropy and spectral break points.

A summary of mean plasma parameters for each period is given in Table 1 together with the anisotropic spectral indices and the mean normalized cross-helicity,  $\sigma_c = (2\mathbf{v} \cdot \mathbf{b})/(\mathbf{v}^2 + \mathbf{b}^2)$ , where  $\mathbf{v}$  and  $\mathbf{b}$  are fluctuations of the velocity and magnetic field in Alfvén units;  $\sigma_c$  is calculated spectrally for the whole of each period, and the values quoted here are means between  $10^{-5}$  and  $10^{-4}$  Hz.  $\sigma_c$  is normalized so that it is positive for Alfvén waves travelling away from the Sun. Its values are consistently above zero, showing the imbalanced nature of the turbulence with a predominance of waves travelling anti-sunward. Values of  $\alpha$  in Table 1, calculated in a fixed range of scales  $2 \times 10^{-2} \leq k\rho_i \leq 2 \times 10^{-1}$  for all five periods, are similar and broadly consistent with  $-5/3$  and  $-2$ , as in the previous section. Due to  $|B|$  and  $\rho_i$  changing this would not be true if we used

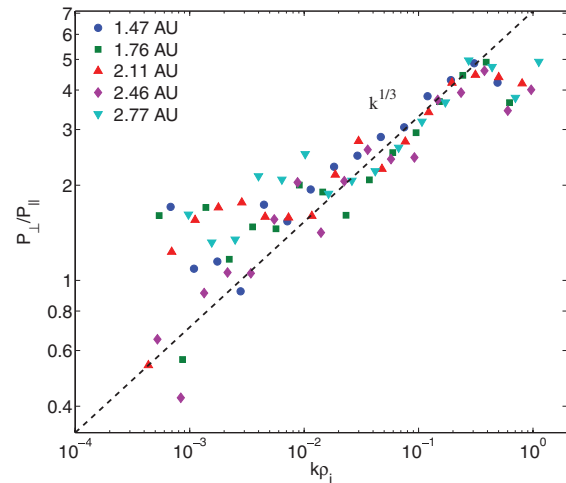


**Figure 3.** Dependence of power anisotropy for each of the five periods in Table 1 on wavenumber scaled to the ion gyroscale,  $k\rho_i$ .

a fixed range of frequencies. This is because as  $\rho_i$  increases with distance from the Sun a set frequency can become comparable to, or smaller than the ion gyroscale, and thus slip into the dissipation range, where the spectra are steeper (e.g. Chen et al. 2010b).

Fig. 3 shows the power anisotropy,  $P_\perp/P_\parallel$ , a quantity introduced by Podesta (2009), as a function of  $k\rho_i$  for the five periods. The data from different periods collapse on to a single line, particularly at larger wavenumbers. Its slope at scales within the inertial range is approximately  $1/3$ , which is the value expected for critically balanced turbulence (Goldreich & Sridhar 1995), because  $k^{-5/3}/k^{-2} = k^{1/3}$ . There is a peak at  $k\rho_i = 0.4$  and a trough at  $k\rho_i = 0.7$ , consistent with fig. 6 of Podesta (2009). For  $k\rho_i < 10^{-2}$ , the values of  $P_\perp/P_\parallel$  mostly rise above the  $k^{1/3}$  line and fill the region  $1 < P_\perp/P_\parallel < 2$ , the region of near-isotropy corresponding to the roll-over to  $\alpha \approx -1$  shown in Fig. 1.

All five periods have a similar peak power anisotropy of  $P_\perp/P_\parallel \approx 5$ . This is close to the value of 7 reported by Podesta (2009) for the fast wind in the ecliptic at 1 au. We note that Podesta (2009) used smaller angular bins than we have here, which could decrease the measured power in the  $P_\parallel$  angle bin, thus increasing the anisotropy.

If we assume a universal anisotropic scaling in the inertial range and take the result shown above, that the outer scale is nearly isotropic, these results imply, perhaps surprisingly, that the total width of the inertial range does not change significantly with distance from the Sun. Indeed Fig. 3 shows that the range of scales from where  $P_\perp/P_\parallel = 1$  to  $k\rho_i = 1$  is always approximately two decades ( $5 \times 10^{-3} \lesssim k\rho_i \lesssim 5 \times 10^{-1}$ ). While, as previous studies have shown (Bavassano et al. 1982; Horbury et al. 1996), both the outer scale and  $\rho_i$  increase with distance from the Sun (Table 1),

**Table 1.** Results from five different periods of Ulysses data from 1995, showing start day and mean physical parameters for each period. The spectral indices of the parallel and perpendicular inertial range are calculated by least-squares fitting of straight lines to the logarithm of the spectra in the range  $2 \times 10^{-2} < k\rho_i < 2 \times 10^{-1}$ .

Start day	R (au)	$ B $ (nT)	$V_{SW}$ (km s $^{-1}$ )	$V_A$ (km s $^{-1}$ )	$n_i$ (cm $^{-3}$ )	$T_i$ (10 $^5$ K)	$\beta_i$	$\sigma_c$	$\rho_i$ (10 $^3$ km)	Inertial range $\alpha$	
										$\alpha(P_\perp)$	$\alpha(P_\parallel)$
100	1.48	2.82	758	56	1.21	2.49	1.35	0.65	1.52	$-1.62 \pm 0.03$	$-1.92 \pm 0.02$
150	1.76	1.98	780	49	0.77	2.09	1.47	0.67	1.98	$-1.58 \pm 0.02$	$-2.00 \pm 0.01$
200	2.11	1.46	785	45	0.50	1.91	1.62	0.58	2.57	$-1.64 \pm 0.01$	$-1.9 \pm 0.1$
250	2.46	1.17	779	41	0.38	1.75	1.77	0.51	3.06	$-1.69 \pm 0.01$	$-1.9 \pm 0.1$
300	2.77	0.97	766	38	0.31	1.61	1.95	0.51	3.56	$-1.64 \pm 0.02$	$-1.94 \pm 0.04$

they increase in such a way as to keep the width of the inertial range approximately constant.

Let us make a simple estimate of how the ratio of  $\rho_i$  and the outer scale ( $L$ ) varies with distance from the Sun  $R$ . We assume  $|B| \propto R^{-1.48}$ ,  $|V| \approx \text{constant}$ ,  $T \propto R^{-1.02}$  and  $L \propto R^{1.1}$ , the scalings that have been obtained from Ulysses observations (Goldstein et al. 1996; Horbury et al. 1996; Ebert et al. 2009). Then

$$\frac{L}{\rho_i} \propto \frac{L|B||V|}{\sqrt{T}} \propto R^{0.13}. \quad (2)$$

This very weak dependence on  $R$  is essentially unmeasurable due to the scatter in the power anisotropy measurements at large scales and the small range of heliocentric distances covered. This explains why we do not see a significant increase in the width of the inertial range.

This simple analysis taken in conjunction with the scaling of the magnetic field strength from the Parker spiral also leads to the conjecture that the inertial range might be wider, closer to the Sun. Close to the Sun  $|B| \propto R^{-2}$ , whereas further out in the heliosphere  $|B| \propto R^{-1}$  (Burlaga et al. 1984, 2002). This would imply  $L/\rho_i \propto R^{-1/2}$  close to the Sun and  $L/\rho_i \propto R^{1/2}$  further out in the heliosphere. The Ulysses results are in the transition region between these two behaviours where the  $L/\rho_i \sim \text{const}$ . Thus, the inertial range in the corona could be wider than that observed here and wider again in the outer heliosphere. The winding of the Parker spiral controls the scaling of the magnetic field magnitude with radius and so this scaling is also dependent on heliospheric latitude.

Finally, we show the similarity between the five periods we analyse and the effect of power enhancement parallel to the field close to the ion gyroradius by plotting compensated spectra for the parallel and perpendicular power. Compensated spectra are defined:

$$P_C(k) = \frac{P(k)}{P_{\perp 0}} \left( \frac{k}{k_0} \right)^{-\alpha}, \quad (3)$$

where  $k_0\rho_i = 2 \times 10^{-1}$  and  $P_{\perp 0} = P_{\perp}(k_0\rho_i)$ , indicated in Fig. 4 by an arrow. The spectral indices used to compensate the spectra are  $\alpha = -5/3$  for the perpendicular spectrum and  $\alpha = -2$  for the parallel spectrum.

Both  $P_{\perp}$  and  $P_{\parallel}$  show a horizontal region between  $2 \times 10^{-2} \lesssim k\rho_i \lesssim 5 \times 10^{-1}$ , implying that the spectral indices are close to

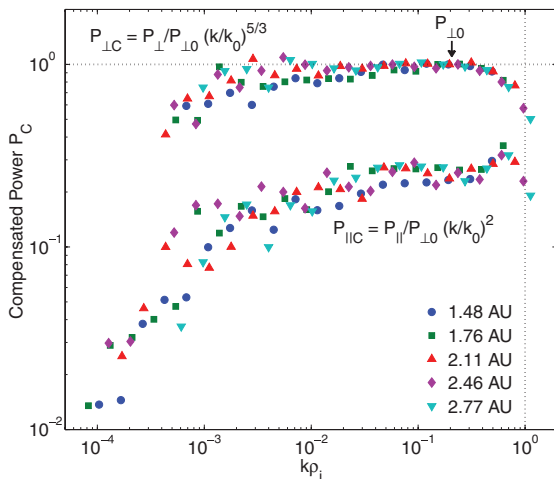


**Figure 4.** Perpendicular and parallel power for each of the five periods in Table 1, compensated to remove a spectral gradient of  $-5/3$  from the perpendicular power and  $-2$  from the parallel.

$-5/3$  and  $-2$  for  $P_{\perp}$  and  $P_{\parallel}$ , respectively. At  $k\rho_i < 10^{-2}$ ,  $P_{\parallel}$  turns downward, the steeper gradient indicating the roll-over towards isotropy and a spectral index of  $-1$  has begun. The outer scale break point is at  $k\rho_i \approx 10^{-3}$ , where another downward turn is seen in both  $P_{\parallel}$  and  $P_{\perp}$ .

At  $k\rho_i \approx 0.7$ , a clear peak can be seen in  $P_{\parallel}$  which coincides with the steepening of  $P_{\perp}$ , similar to that noted by Podesta (2009). This peak is remarkably consistent across all five periods used. The  $P_{\parallel}$  peak suggests a local enhancement (and perhaps injection) of energy possibly due to ion kinetic instabilities, but does not of course prove it. Ulysses high speed wind particle distributions are often close to the firehose instability threshold (Matteini et al. 2007, see also Hellinger & Trávníček 2008). The enhancement appears to be in fluctuations whose wavevectors are parallel to the field. This enhancement in  $P_{\parallel}$  is approximately an order of magnitude smaller than  $P_{\perp}$  at this scale. A change of this size would be difficult to detect in  $P_{\perp}$ , so we cannot rule out the possibility that the excited wavevectors might be oblique. What is clear is that the anisotropy is reduced at this scale, perhaps by an admixture of fluctuations with  $k_{\parallel} \geq k_{\perp}$ .

Note that the peak in  $P_{\parallel}$  is at the same  $k\rho_i$  for all spectra, despite the fact that frequencies and power levels change significantly over the five periods used. This means that what we see is a physical effect associated with the gyroscale and not an instrumental or spacecraft effect. If the ion inertial length is used instead of the ion gyroscale to normalize the wavenumber axis, this peak is not as well defined.

## 5 CONCLUSIONS

We have used a wavelet analysis of Ulysses fast polar solar wind observations to study the anisotropy of the entire inertial range of turbulence with respect to the local mean magnetic field. Our analysis shows that turbulence is isotropic at the outer scale. The spectral index is approximately  $-1$  for scales larger than the outer scale.

At scales smaller than the outer scale, the turbulence develops a spatial anisotropy with lower power in magnetic field fluctuations that vary along the local mean magnetic field and a corresponding spectral index of  $-2$ , while the higher power in cross-field fluctuations has a  $-5/3$  spectrum. These magnetic field spectral scalings are consistent with a critically balanced Alfvénic cascade (Goldreich & Sridhar 1995). The perpendicular scaling appears closer to  $-5/3$  than to  $-3/2$  predicted by some theories (Boldyrev 2006) and found in numerical simulations (e.g. Maron & Goldreich 2001).

The width of the inertial range remains approximately constant at all heliocentric distances investigated. This can be understood by considering the change in the ratio of outer scale to the ion gyroscale with heliocentric distance and leads to the conjecture that the inertial range is wider, closer to the Sun and in the outer heliosphere (see Section 4). The small scale end of the inertial range seems naturally to scale with ion gyroradius. There appears to be an injection of power into parallel wavenumbers at  $k\rho_i \sim 1$ , conceivably due to the firehose instability.

Our results show yet again that the solar wind is a unique laboratory for studying plasma turbulence across a wide range of scales in extraordinary detail. The isotropy at the outer scale and the remarkable consistency of the behaviour at the ion gyroscale show that solar wind turbulence is not only interesting for its own sake, but also as a representative case study of a magnetized plasma of the kind that is ubiquitous in the Universe.

## ACKNOWLEDGMENTS

We thank M. Forman, P. Hellinger and L. Matteini for useful discussions. This work was funded by STFC and by the Leverhulme Trust Network for Magnetized Plasma Turbulence.

## REFERENCES

- Alexandrova O. et al., 2008, *ApJ*, 674, 1153  
 Balogh A. et al., 1992, *A&AS*, 92, 221  
 Bavassano B., Dobrowolny M., Mariani F., Ness N. F., 1982, *J. Geophys. Res.*, 87, 3617  
 Beresnyak A., Lazarian A., 2009, *ApJ*, 702, 460  
 Bieber J., Wanner W., Matthaeus W. H., 1996, *J. Geophys. Res.*, 101, 2511  
 Boldyrev S., 2006, *Phys. Rev. Lett.*, 96, 115002  
 Burlaga L. F., Klein L. W., Lepping R. P., Behannon K. W., 1984, *J. Geophys. Res.*, 89, 10659  
 Burlaga L. F., Ness N. F., Wang Y.-M., Sheeley N. R. Jr, 2002, *J. Geophys. Res.*, 107, 1410  
 Chandran B. D. G., 2008, *ApJ*, 685, 646  
 Chapman S. C., Hnat B., 2007, *Geophys. Res. Lett.*, 34, L17103  
 Chen C. H. K., Wicks R. T., Horbury T. S., Schekochihin A. A., 2010a, *ApJ*, 711, L79  
 Chen C. H. K. et al., 2010b, *Phys. Rev. Lett.*, 104, 255002  
 Dasso S., Milano L. J., Matthaeus W. H., Smith C. W., 2005, *ApJ*, 635, L181  
 Ebert R. W. et al., 2009, *J. Geophys. Res.*, 114, A01109  
 Goldreich P., Sridhar S., 1995, *ApJ*, 438, 763  
 Goldstein M. L., Roberts D. A., Matthaeus W. H., 1995, *ARA&A*, 33, 283  
 Goldstein B. E., Neugebauer M., Phillips J. L. et al., 1996, *A&A*, 316, 296  
 Hellinger P., Trávníček P. M., 2008, *J. Geophys. Res.*, 113, A10109  
 Horbury T. S., Balogh A., Forsyth R. J., Smith E. J., 1996, *A&A*, 316, 333  
 Horbury T. S., Forman M. A., Oughton S., 2008, *Phys. Rev. Lett.*, 101, 175005  
 Lithwick Y., Goldreich P., Sridhar S., 2007, *ApJ*, 655, 269  
 Maron J., Goldreich P., 2001, *ApJ*, 554, 1175  
 Matteini L. et al., 2007, *Geophys. Res. Lett.*, 34, L20105  
 Matthaeus W. H., Oughton S., Pontius D. H. Jr, Zhou Y., 1994, *J. Geophys. Res.*, 99, 19267  
 Milano L. J., Dasso S., Matthaeus W. H., Smith C. W., 2004, *Phys. Rev. Lett.*, 93, 155005  
 Nicol R. M., Chapman S. C., Dendy R. O., 2009, *ApJ*, 703, 2138  
 Osman K. T., Horbury T. S., 2007, *ApJ*, 654, L103  
 Perez J. C., Boldyrev S., 2009, *Phys. Rev. Lett.*, 102, 025003  
 Podesta J. J., 2009, *ApJ*, 698, 986  
 Sahraoui F., Goldstein M. L., Robert P., Khotyaintsev Y. V., 2009, *Phys. Rev. Lett.*, 102, 231102  
 Schekochihin A. A. et al., 2009, *ApJS*, 182, 310  
 Taylor G. I., 1938, *Proc. Roy. Soc.*, 164, 476  
 Tessein J. A. et al., 2009, *ApJ*, 692, 684  
 Torrence C., Compo G. P., 1998, *Bull. Am. Meteorological Soc.*, 79, 61  
 Weygand J. M. et al., 2009, *J. Geophys. Res.*, 114, A07213

This paper has been typeset from a  $\text{\TeX}/\text{\LaTeX}$  file prepared by the author.